https://doi.org/10.18321/ectj697

Composition and Corrosion Behavior of Iron-Cobalt-Tungsten

M. Ved'[1], N. Sakhnenko[1], I. Yermolenko[1], G. Yar-Mukhamedova[2*], R. Atchibayev[2]

[1]National Technical University "Kharkiv Polytechnic Institute" 2, Kyrpychova str., 61002, Kharkiv, Ukraine
[2]Al-Farabi Kazakh National University, IETP, al-Farabi ave. 71, 050040 Almaty, Kazakhstan

Article info

Received:
6 July 2017

Received in revised form:
27 September 2017

Accepted:
24 January 2018

Abstract

Principles of three component Iron-Cobalt-Tungsten alloys electrodeposition from complex Fe (III) based citrate electrolytes are discussed. It is shown, that deposition of ternary alloys proceeds through competitive reduction of cobalt and tungsten with iron. With increasing ligand concentration coatings are enriched with a refractory component; however, increasing current density favors a reverse trend. The effect of both current density and pulse on/off time on the quality, content of alloying metals and surface topography of electrolytic coatings were determined. The application of pulsed electrolysis provides increasing tungsten content up to 13 at.%, at current efficiency of 70–75%. Globular relief of Fe-Co-W coatings is caused by refractory metals incorporation, and crystalline and amorphous parts of structure are visualized by X-ray spectroscopy, including inter-metallic phases Co_7W_6, Fe_7W_6 along with α-Fe and Fe_3C. The crystallite size of the amorphous part is near 7–8 nm. Corrosion resistance of the coatings is 1.3–2.0 orders of magnitude higher than the substrate parameters as follows from data of polarization resistance method and electrode impedance spectroscopy.

1. Introduction

Interest to the electrolytic multi-component alloys is due to extended functional properties of such materials which exceed performance of separate metals. Special place belongs to the alloys of iron family metals with refractory elements [1–3]. Spheres of multi-component coatings application are replacement of electrolytic toxic chromium and hardening of the surface [4–9], corrosion protection [10, 11], magnetic films with increased microhardness [12, 13], catalytic materials for heterogeneous red-ox processes [14, 15] and for electrodes in fuel cells (FC) and various red-ox flow batteries (RFB) [16–21].

Utilization of the electrochemical methods for thin alloy coatings synthesis displays interactions in the chain "process parameters – composition and structure of the material – properties – functions – application" [5]. Of course, the advantage of above techniques for deposition thin-film multi-component systems is the possibility to operate the deposition rate and improve adhesion to the substrate; to direct the relief of a surface and distribution of alloying elements using simple approaches and technique such as variation of the electrolytes composition and polarization modes namely different type of current [22–26].

Prior and current publications mainly reflect the features of deposition and properties of two component Fe(Ni, Co)-Mo(W) alloys, but there are some positive results of the multi-component alloys deposition from the gluconate-chloride [4], citrate and citrate-ammonia [27], pyrophosphate [28], sulfate-citrate [29] electrolytes in galvanostatic and non-stationary mode. However, the main problem of the presented technologies remains the low content of refractory components and current efficiency [30, 31].

Given this, a study of effect of electrolyte composition and parameters of pulse current on the components content and surface state and, consequently, properties of electrodeposited Fe-Co-W coatings is topical.

*Corresponding author. E-mail: gulmira-alma-ata@mail.ru

2. Experimental

Ternary coatings were deposited onto planar samples out of two metals: copper and mild steel. Pretreatment of copper samples surface included mechanical polishing, degreasing, chemical etching in a mixture of the 50% nitric and 50% sulfuric acids, thorough washing with distilled water and drying as in [32]. Processing of steel samples before electrodeposition consists of the following operations: sanding with sandpaper number 0, degreasing in an alkali solution at 50 °C, and washing, etching in a mixture of middle concentration HCl/H_2SO_4 at volume ratio 1/1 at a room temperature, and thoroughly washing.

Fe-Co-W coatings were formed from electrolytes of the composition provided in Table 1 as was proposed in [22]. The acidity of solution was not specially changed, it was set by the ratio of the electrolyte components at pH of 4.3–4.6.

All electrolytes were prepared from analytically pure reagents, separately dissolved in distilled water added with citrate ligand, and then were mixed in a specific order as was discussed in [33–35]. The acidity of solutions was controlled by pH-meter. Electrolyte temperature during deposition was varied in the range of 25–35 °C.

The Fe-Co-W coatings were deposited using: (i) direct current of density i 2–7 A/dm^2 and (ii) pulse current of amplitude i of 2–6 A/dm^2 at pulse duration (on-time) ton 10–20 ms and pause duration (off-time) t_{off} 10–50 ms. Planar electrodes of AISI 304 steel were anodes; the cathode-to-anode area ratio was 1 : 5, volume current density was 2 A/dm^3.

The current efficiency Ce (%) of electrolysis and thickness of the coatings were calculated from the change in samples weight after deposition taking into account the electrochemical equivalent of the alloy.

The character and topography of the deposits' surface was analysed with a Zeiss EVO 40XVP scanning electron microscope (SEM). Images were recorded by the registration of secondary electrons (SEs) via scanning with an electron beam to obtain a high resolution and contrast ratio. The elements' content in the coatings was determined using EDS method by an Oxford INCA Energy 350 unit integrated into the system of the SEM using electrons' beam of 15 keV.

The topography of thin films' surface was studied by an atomic force microscopy AFM using a NT–206 scanning probe. Scanning was performed using the contact probe CSC-37 with a cantilever lateral resolution of 3 nm [36]. In order to analysis the AFM images, all image data were converted into Surface Explorer software.

The phase structure of the deposits was examined by X-ray diffraction analysis using a diffractometer (DRON-2.0) in the emission of cobalt anode. X-ray patterns were recorded in discrete mode with a step $2\theta = 0.1$ ° with the exposure at each point for 20 sec; operating voltage was 35 kV, and current 20 mA. The size of the coherent scattering regions (L) was determined from the half-width ($P_{1/2}$) of the diffraction line at small angles θ by the Selyakov-Scherer formula:

$$L = \lambda/(P_{1/2}\cos\theta),$$

where λ – wavelength of used radiation.

Corrosion behavior of coated samples was studied in model media of different aggressiveness, namely 1 M Na_2SO_4 acidified to pH 3(i), alkalized to pH 11 (ii), and in 3% NaCl (pH 7). Polarization resistance method based on the analysis of Tafel's anodic and cathodic plots within the range of 200–300 mV from open circuit potential was used to estimate the corrosion current [37]. Polarization dependences were registered by IPC-Pro unit controlled by PC with potential scanning rate of 1 mV/sec. Corrosion depth index k_h (mm per year) was calculated from corrosion current as in [38]:

$$k_h = (8.76 k_e i_{cor})/\rho,$$

where k_e – the electrochemical equivalent of alloy, kg·C^{-1}; i_{cor} – corrosion current density, A/m^2; ρ – density of the alloy, kg/m^3.

The results were verified by spectroscopy of electrode impedance SEI in solution 2% NaCl. SEI was recorded in a two-electrode cell on electrodes of 1 cm^2, located planar at a distance of 1 cm apart using module Autolab-30 (model PGSTAT301N Metrohm Autolab) with module FRA-2 (Frequency Response Analyzer) in frequency range 10^{-2} – 10^6 Hz. Module management was performed using Autolab 4.9 under the standard procedure, followed by processing of the data in the Zview 2.0 package. The modeling of the structure and the state of the phase boundary was performed by the method of equivalent substitution schemes. Parameters with an error in simulating an equivalent circuit of not more than 10% are taken into consideration. Measurements are carried out at temperature 18±1 °C.

Table 1
Electrolytes for deposition Fe-Co-W coating

Components concentration, mol/dm³	The ratio $c(Fe^{3+}) : c(Co^{2+}) : c(WO_4^{2-}) : c(Cit^{3-})$	
	1	2
	1 : 1.3 : 0.6 : 2.7	1 : 1.3 : 0.6 : 2.7
Iron (III) sulfate	0.075	0.075
Cobalt sulfate	0.2	0.2
Sodium tungstate	0.06	0.06
Sodium citrate	0.4	0.5
Sodium sulfate	0.15	0.15
Boric acid	0.1	0.1
pH	4.3	4.55

3. Results and discussion

The electrolyte pH increases (Table 1) if we rise the concentration of citrate ions in the solution at fixed Fe^{3+} content. The protonation of citrate anions decreases with pH, as well as degree of Fe^{3+} hydrolysis increasing, therefore ionic forms of complexing agents and ligand in the electrolytes are different. Consequently, the composition of particles discharged at the electrode varies, which effect the composition of coatings.

Cathodic reduction of separate metals in Fe-Co-W alloy occurs by competition between Iron, Cobalt and Tungsten [27, 33, 35]. The order of competition depends on the ratio of alloying components' concentration in electrolyte, and also on the electrolysis mode and parameters (Fig. 1). We observed a decrease in the cobalt and tungsten content in favor the iron portion in the alloy at all current densities (Fig. 1a), if the ratio of electrolyte components concentration $c(Fe^{3+}) : c(Co^{2+}) : c(WO_4^{2-}) : c(Cit^{3-})$ is 1 : 1.3 : 0.6 : 2.7 (electrolyte 1, Table 1). This occurs as a result of competitive reduction of alloying components from hetero-nuclear complexes. The cobalt content exceeds the iron portion in coatings deposited at current densities of 3–7 A/dm². A trend to gradually decreasing the cobalt content is observed with increasing current density (Fig. 1a). Iron and cobalt are co-deposited in the alloy in the ratio 1 : 1 at a current density of 6 A/dm². Further rising i_c promotes a significant increase in iron content at the expense of cobalt and tungsten. The refractory component content in the alloy varies within 8–10 at.% with tendency to decrease at rising current density. It should be noted that iron, cobalt and tungsten are co-deposited at the alloy in proportion to 4.5 : 5 : 1 respectively, if alloying metals ratio in the electrolyte is $c(Fe^{3+}) : c(Co^{2+}) : c(WO_4^{2-}) = 2.5 : 3 : 1$.

Tungsten content increases slightly (9–11 at.%) if the citrate concentration in the solution is 0.5 mol/dm³ other things being equal (Fig. 1b). However, the trend to tungsten content decreasing with rising current density is maintained. At the same time, the competitive reduction of iron and cobalt becomes more significant. The iron content in the coating increases to 59 at.% with a simultaneous decreasing in cobalt portion to 30 at.% when rising current density from 3 A/dm² to 7 A/dm² as we can see from Fig. 1b.

The efficiency of galvanostatic deposition does not exceed 45%, regardless of the electrolyte concentration. Increasing i_c to 7 A/dm² reduces the current efficiency to 27% due to side reaction of hydrogen evolution. Deposited in stationary mode Fe-Co-W coatings have globular morphology of surface with a grain sizes of 2–6 μm (Fig. 2a). Coatings deposited in pulse mode contain higher amounts of refractory metals, and are more uniform (Fig. 2b). The tungsten content in the coatings deposited by pulse current from electrolyte 2 (Table 1) is of 12.5 at.%. On more developed surface of enriched with tungsten coatings, we can see agglomerates of spheroids (Fig. 2c).

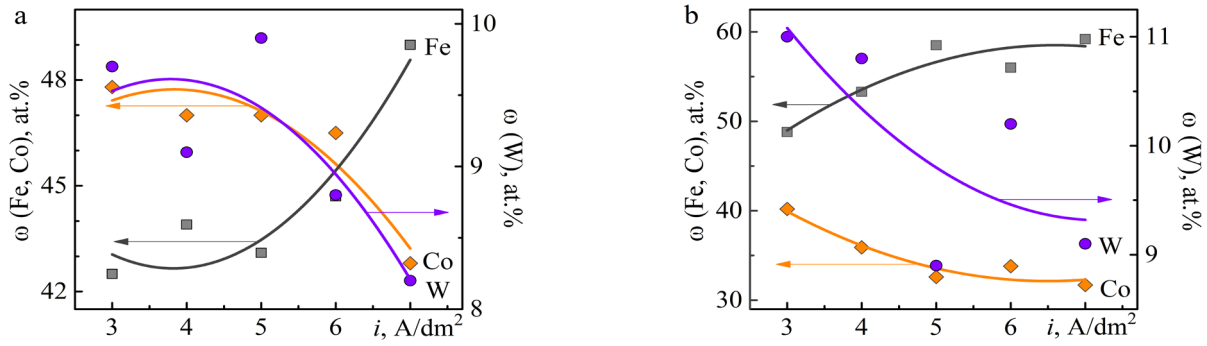

Fig. 1. Current density effect on Fe-Co-W coatings composition deposited from electrolytes: 1 (a) and 2 (b). The error bars for W are within 0.5%, for other metals – 1.0%.

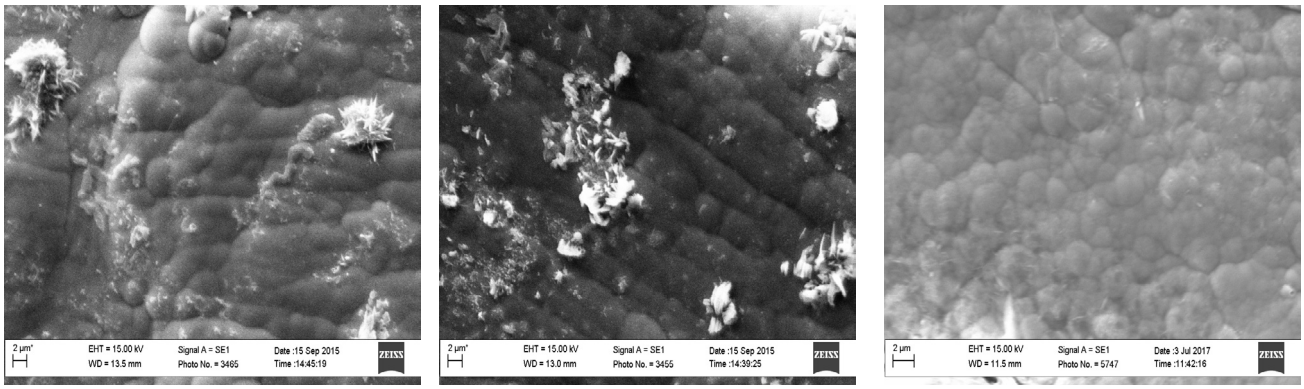

(a) (b) (c)

Fig. 2. The morphology and composition (at.%) of Fe-Co-W coatings deposited from electrolytes: 1 (a, b), 2 (c) in galvanostatic (a) and pulse (b, c) modes – a – i = 3 A/dm^2; b – i = 3 A/dm^2, t_{on}/t_{off} = 50/50 ms; c – i = 5 A/dm^2, t_{on}/t_{off} = 20/20 ms.

Time parameters of pulsed electrolysis are an effective tool for controlling the composition and nature of the coating surface. Prolong pulse at a fixed pause time contributes an increasing of cobalt and tungsten content in the alloy at studied current densities (Fig. 3). At the same time, observed for the galvanostatic regime rising trend of iron content at the expense of cobalt and tungsten with increasing current density is preserved, as one can see on Fig. 3a, b.

The deposition efficiency increases almost twice when applying pulse current as compared with galvanostatic regime: at i = 3 A/dm^2 the efficiency of electrolysis is of 70–75%, and at i = 4 A/dm^2 Ce decreases to 63–68%, due to site hydrogen evolution reaction.

The roughness of deposited alloys Fe-Co-W containing tungsten of 10–12 at.% was compared with surface of polished mild steel substrate. The surface of substrate (Fig. 4) is fairly uniform and not ordered; and roughness indices at scan area 5.0×5.0 µm are detected as Ra = 0.008 and Rq = 0.011. We can see from Fig. 4 that surface cross-section profile between points 1 and 2 indicates the spheroidal agglomerates sizes to be of 2–3 µm.

The surface of three component coatings Fe-Co-W deposited at polished steel becomes more globular compared with substrate, and contains spheroid and cone-shaped agglomerates (Figs. 4 and 5) as follows from AFM analysis in the frame of same scanning area. One can see that larger spheroid agglomerates of 2.5–3.5 µm are formed with a smaller cone-shaped grains of 0.2–0.5 µm in diameter (Fig. 5). It was shown the influence of refractory metals incorporation in alloy on the morphology and development of a surface [3, 7, 11] and consequently microhardness, corrosion resistance, and catalytic activity of the material [4, 15, 21]. The surface roughness parameters of Fe-Co-W deposits at scanning area 5×5 µm are defined as Ra = 0.06 and Rq = 0.07 that much higher than those for the substrate that indicates substantial development of the surface.

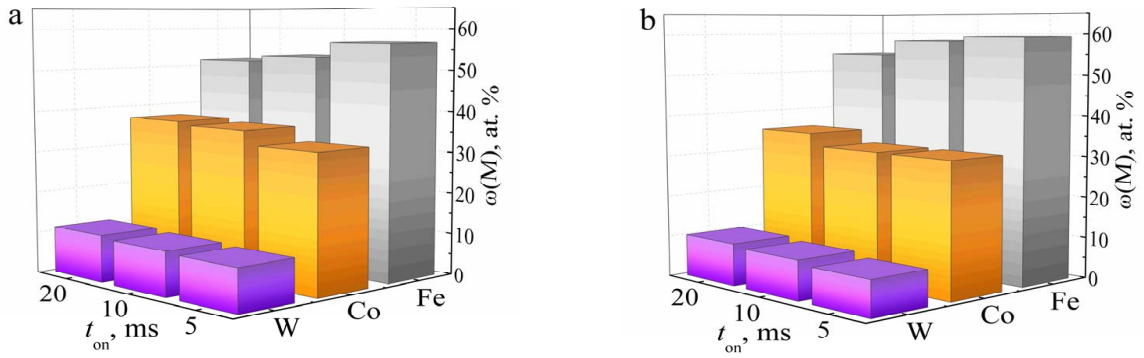

Fig. 3. Pulse duration effect on the composition Fe-Co-W alloy deposited from electrolyte W_2 at t_{off} = 10 ms; current density i, A/dm^2: a – 5, b – 6.

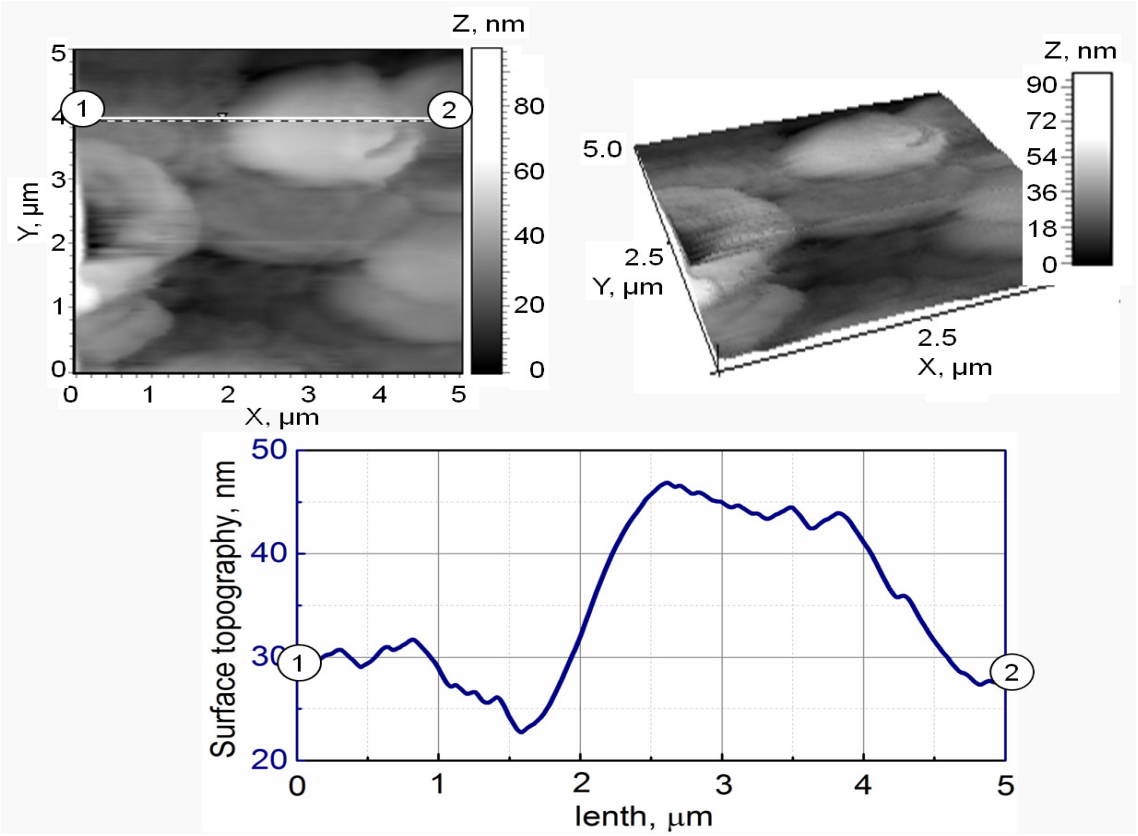

Fig. 4. Mild steel substrate: 2D- and 3D maps of the surface and cross section profile between points 1 and 2 at scan area 5.0×5.0 μm.

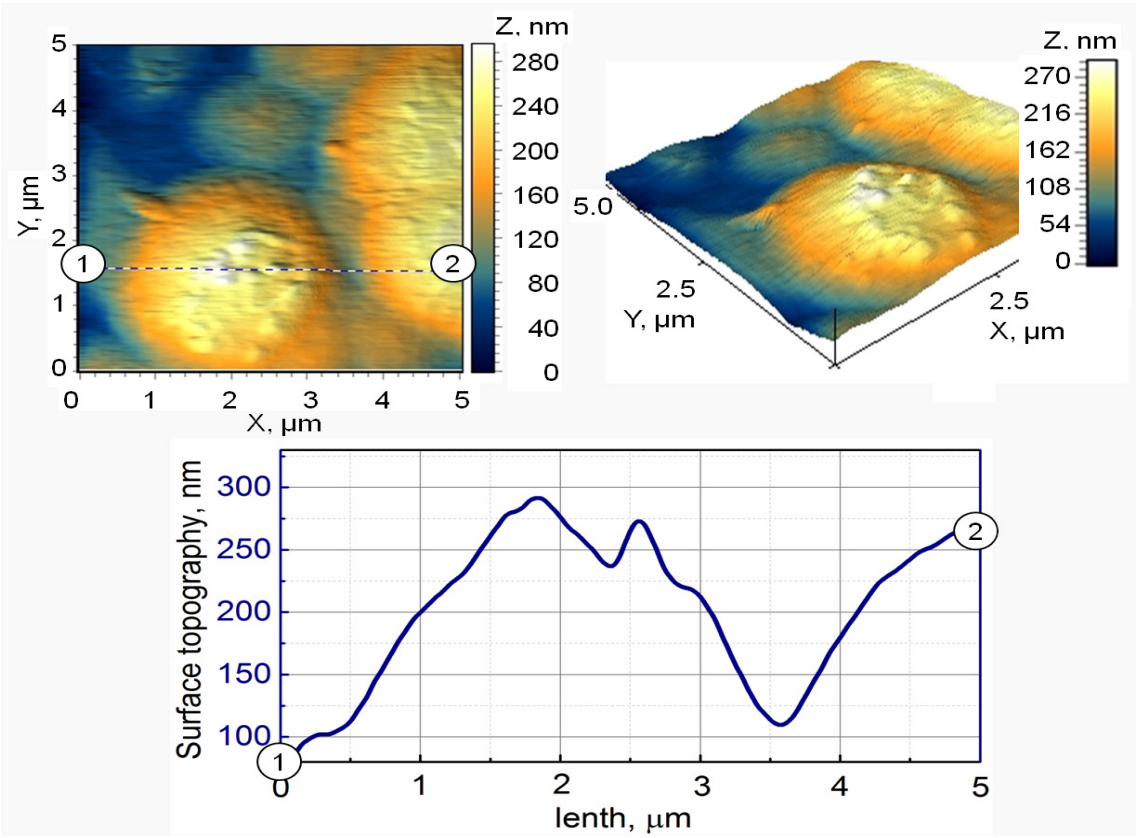

Fig. 5. 2D-, 3D-map and cross section profile between points 1–2 for coating Fe-Co-W deposited at pulse current of 4 A/dm^2; t_{on}/t_{off} = 10/10 ms; T = 25 °C; pH 4.3; plated time 30 min. Scan area 5.0×5.0 μm.

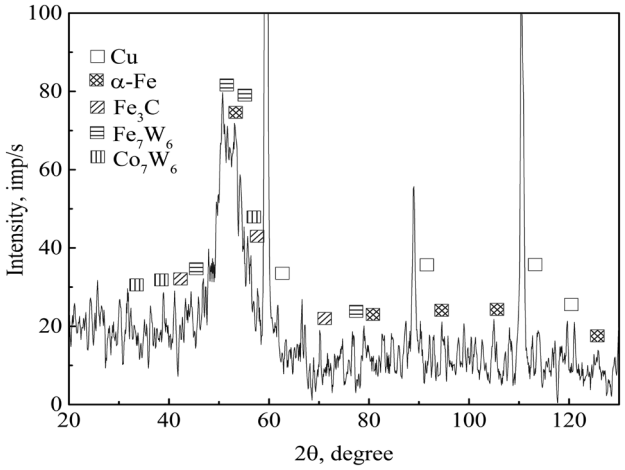

Fig. 6. X-ray diffraction patterns for deposit Fe-Co-W, the composition is similar to Fig. 2b.

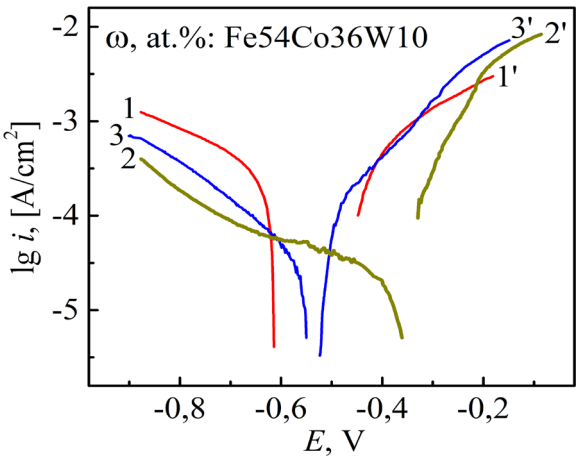

Fig. 7. The cathodic (1, 2, 3) and anodic (1', 2', 3') polarization dependences of the coatings in corrosive environment with pH 3 (1, 1'), pH 5 (2, 2') and pH 9.5 (3, 3').

Figure 6 shows the results of X-ray diffraction analysis and phase structure for Fe-Co-W coatings (thickness 30 μm) containing at.%: Fe – 58.4, Co – 35.4, W – 6.2, deposited on substrate made of copper. The X-ray diffraction pattern indicates Fe-Co-W deposits to be amorphous-crystalline (Fig. 6). We can see some lines of copper substrate, and lines corresponding to inter-metallic phases Co_7W_6 and Fe_7W_6, as well as α-Fe and cementite Fe_3C at diffraction patterns. Besides, a low halo with width about 10º is detected at angles 2θ 50–55º (Fig. 6), that corresponds to amorphous structure. The crystallite size of the amorphous part is 8 nm.

Phases Co_7W_6, Fe_7W_6, α-Fe and Fe_3C found in Fe-Co-W deposits, reflect the competition of alloying metals reduction from hetero-nuclear complexes, and confirm mechanism of co-deposition proposed in [23, 34].

Corrosion of cobalt based electrolytic coatings as it follows from the nature of alloying components proceeds predominantly with hydrogen depolarization in an acidic medium (Fig. 7), and oxygen is a depolarizer in neutral and alkaline media. The open circuit potential of Fe-Co-W coatings becomes more negative compared with steel in all examined solution. Such behavior may be attributed with the cathodic control of the corrosion process.

The cathode reaction is inhibited due to the depolarizer (oxygen) transport deceleration caused by acidic non-stoichiometric tungsten oxides. Thus, the coatings enrichment with tungsten, which occurs predominantly at the expense of iron content, contributes increasing corrosion resistance in acidic media. Corrosion current decreasing in a neutral media indicates the formation and stability of alloying components passive oxide film, even in the presence of activating Cl– ions. In the alkaline media, on the contrary, the cathode reaction inhibition is ensured by insoluble iron hydroxides formed on the alloy surface, which prevent depolarizer transport to the substrate. The highest corrosion resistance in alkaline medium is observed for three component Fe-Co-W coatings containing 59 at.% Iron and 8 at.% Tungsten (Table 2).

The Nyquist plots for Fe-Co-W alloy is a connection of two conjugate semicircles with different time constants τ = RC (Fig. 8a), that reflects the presence of two phases and, respectively, two boundaries, which can be attributed as: 1 – electrolyte/oxide on the surface of the electrode; 2 – electrolyte/metal.

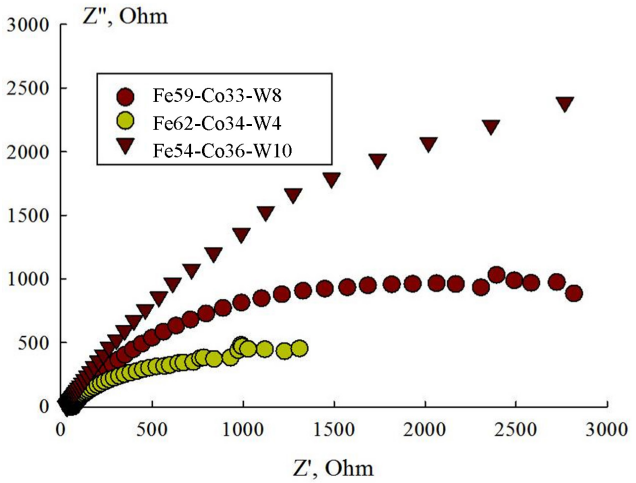

Fig. 8. The Nyquist plots for steel electrode and Fe-Co-W alloys in a neutral chloride-containing environment.

Table 2
Corrosion indices of steel substrate and Fe-Co-W coatings

Composition of alloy, ω, at.%	pH 3		pH 5		v	
	E_{cor}, V	lg i_{cor}, A/cm^2	E_{cor}, V	lg i_{cor}, A/cm^2	E_{cor}, V	lg i_{cor}, A/cm^2
Steel	–0.34	–2.8	–0.35	–3.0	–0.32	–2.8
Fe54Co36W10	–0.54	–4.7	–0.36	–5.1	–0.53	–5.2
Fe59Co33W8	–0.35	–4.1	–0.39	–4.8	–0.36	–5.5

The equivalent scheme (Fig. 8b) contains the elements: R1 is the resistance of the electrolyte, L1 is the inductive component of the impedance, CPE1 is the capacity of the inter-phase boundary electrolyte/oxide on the electrode surface, R2 is the resistance of the oxide layer, CPE2 is the capacity of inter-phase boundary electrolyte/metal and R3 is resistance, equivalent to corrosion resistance R_{cor}. The resistance of inductance L1 is due to the appearance of galvano-magnetic Hall effects at high frequencies and associated with the magnetic properties of the coatings, as well as forming metals oxide films, which differ in specific resistance and capacity and cause several conduction paths. Parameter R_{cor} for tested materials decreases in the range: R_{cor}(Fe-Co-W10) > R_{cor}(Fe-Co-W8) >> R_{cor}(steel).

The relatively near values of the corrosion current density, calculated from data of polarization resistance technique and EIS, are also evidence of correctness both the parameters of corrosion process determination, and the validity of the electrochemical systems equivalent circuit.

4. Conclusions

(i) Thus ternary Fe-Co-W alloys with micro-globular surface of different composition were deposited by direct and pulse current from citrate Fe(III) based electrolyte. Current density and time parameters of pulse electrolysis are shown to be affective tools to control the refractory metals content and electrolysis efficiency.

(ii) Micro-globular surface of Fe-Co-W alloys is caused by tungsten incorporation. It was found the amorphous-crystalline structure of deposits with crystallite sizes of the amorphous part equal to 8 nm.

(iii) Deposited coatings are characterized by increased corrosion resistance in acidic environment due to the acidic nature of refractory oxide components, in neutral resistance to pitting corrosion, which generally exceeds the chemical resistance of substrates and binary coatings.

Acknowledgments

This work was supported by al-Farabi Kazakh National University, Institute of Experimental & Theoretical Physics by AP05130069 project "Development of nanotechnology for the synthesis of functional galvanic coatings for electrical equipment components".

References

[1]. N. Tsyntsaru, H. Cesiulis, M. Donten, J. Sort, E. Pellicer, E.J. Podlaha-Murphy, *Surf. Engin. Appl. Electrochem.* 48 (6) (2012) 491–520. DOI: 10.3103/S1068375512060038

[2]. E.J. Podlaha, D. Landolt, *J. Electrochem. Soc.* 144 (5) (1997) 1672–1680. DOI: 10.1149/1.1837658

[3]. G. Yar-Mukhamedova, M. Ved', N. Sakhnenko, A. Karakurkchi, I. Yermolenko, *Appl. Surf. Sci.* 383 (2016) 346–352. DOI: 10.1016/j.apsusc.2016.04.046

[4]. H. Capel, P.H. Shipway, S.J. Harris, *Wear* 255 (2003) 917–923. DOI: 10.1016/S0043-1648(03)00241-2

[5]. M.V. Ved', M.D. Sakhnenko, H.V. Karakurkchi, I.Yu. Ermolenko, L.P. Fomina, *Mater. Sci.* 51 (5) (2016) 701–710. DOI: 10.1007/s11003-016-9893-5

[6]. H. Feng-jiao, L. Jing-tian, L. Xin, H. Yu-ning, *Trans. Nonferrous Met. Soc. China* 14 (5) (2004) 901–906.

[7]. G. Yar-Mukhamedova, M. Ved', N. Sakhnenko, *Appl. Surf. Sci.* 421 (2017) 68–76. DOI: 10.1016/j.apsusc.2017.01.196

[8]. S.A. Silkin, A. Gotelyak, N. Tsyntsaru et al Proceedings of the 8th International Scientific Conf. "BALTTRIB 2015". (2016) 51–56.

[9]. L. Ma, X. Xi, Z. Nie, T. Dong, Y. Mao, *Int. J. Electrochem. Sci.* 12 (2017) 1034–1051. DOI: 10.20964/2017.02.37

[10]. N. Tsyntsaru, A. Dikusar, H. Cesiulis, J.-P. Celis, Zh. Bobanova, S. Sidel'nikova, S. Belevskii, Yu. Yapontseva, O. Bersirova, V. Kublanovskii, *Powder Metall. Met. Ceram.* 48 (7-8) (2009) 419–428. DOI: 10.1007/s11106-009-9150-7

[11]. Y.S. Yapontseva, A.I. Dikusar, V.S. Kyblanovskii, *Surf. Engin. Appl. Electrochem.* 50 (2014) 330–336. DOI: 10.3103/S1068375514040139

[12]. E. Gomez, E. Pellicer, E. Valles, *J. Electroanal. Chem.* 517 (2001) 109–116. DOI: 10.1016/S0022-0728(01)00682-9

[13]. E. Gómez, E, Pellicer, E, Vallés, *J. Electroanal. Chem* 568 (2004) 29–36. DOI: 10.1016/j.jelechem.2003.12.032

[14]. V.S. Kublanovsky, Yu.S. Yapontseva, *Electrocatalysis* 5 (2014) 372–378. DOI: 10.1007/s12678-014-0197-y

[15]. M. Glushkova, T. Bairachna, M. Ved, M. Sakhnenko, In MRS Proceedings. Cambridge University Press. 12 (2013) 1491.

[16]. J. Larminie, A. Dicks Fuel cell systems explained, 2nd ed. John Wiley & Sons Ltd, Chichester (2003) 121–137.

[17]. G. Yar-Mukhamedova, A. Darisheva, K. Kasimzhanov, D. Babazhanov, B. Barkitova, *Eurasian Chemico-Technological Journal* 17 (2015) 209–212. DOI: 10.18321/ectj246

[18]. M. Skyllas-Kazacos, M.H. Chakrabarti, S.A. Hajimolana, F.S. Mjalli, and M. Saleem, *J. Electrochem. Soc.* 158 (2011) 55–79. DOI: 10.1149/1.3599565

[19]. S.M. Haile, *Acta Mater.* 51 (2003) 5981–6000. DOI: 10.1016/j.actamat.2003.08.004

[20]. N. Sakhnenko, M. Ved, Y. Hapon, T. Nenastina, *Russ. J. Appl. Chem.* 88 (2015)1941–1945. DOI: 10.1134/S1070427215012006X

[21]. E Vernickaite, N Tsyntsaru, H. Cesiulis, *Surface and Coatings Technology* 307 (2016) 1322-1328. DOI: 10.1016/j.surfcoat.2016.07.049

[22]. I.Y. Yermolenko, M.V. Ved, N.D. Sakhnenko, Y.I. Sachanova, *Nanoscale Res. Lett.* 12(1) (2017) 352. DOI: 10.1186/s11671-017-2128-3

[23]. M.V. Ved', N.D. Sakhnenko, A.V. Karakurchi, S.I. Zyubanova, *Russ. J. Appl. Chem.* 87 (2014) 276−282. DOI: 10.1134/S1070427214030057

[24]. I. Shao, P.M. Vereecken, C.L. Chien, R.C. Cammarata, and P.C. Searson, *J. Electrochem. Soc.* 150 (2003) 184–188. DOI: 10.1149/1.1553789

[25]. N. Tsyntsaru, H. Cesiulis, A. Budreika, X. Ye, R. Juskenas, J.-P.Celis, *Surface and Coatings Technology* 206 (2012) 4262–4269. DOI: 10.1016/j.surfcoat.2012.04.036

[26]. D.Z. Grabco, I.A. Dikusar, V.I. Petrenko, E.E. Harea, O.A. Shikimaka, *Surf. Engin. Appl. Electrochem.* 43 (2007) 11–17. DOI: 10.3103/S1068375507010024

[27]. A.V. Karakurkchi, M.V. Ved', N.D. Sakhnenko, I.Yu. Ermolenko, *Russ. J. Appl. Chem.* 88 (2015) 1860−1869. DOI: 10.1134/S107042721501101 8X

[28]. N Elezović, B.N. Grgur, N.V. Krstajić, and V.D. Jović, *J. Serb. Chem. Soc.* 70(6) (2005) 879–889. DOI: 10.2298/JSC0506879G

[29]. E. Gomez, E. Pellicer, X. Alcobe, E. Valles, *J. Solid State Electrochem.* 8 (2004) 497–504. DOI: 10.1007/s10008-004-0495-z

[30]. F.I. Danilov, I.V. Sknar, Yu.E. Sknar, *Russ. J. Electrochem.* 50 (2014) 293–296. DOI: 10.1134/S1023193514030045

[31]. D.P. Weston, S.J. Harris, P.H. Shipway, N.J. Weston, G.N. Yap, *Electrochim. Acta* 55 (2010) 5695–5708. DOI: 10.1016/j.electacta.2010.05.005

[32]. G.Sh. Yar-Mukhamedova, N.D. Sakhnenko, M.V. Ved', I.Yu. Yermolenko and S.I. Zyubanova, *IOP Conf. Series: Materials Science and Engineering* 213 (2017) 012019 DOI: 10.1088/1757-899X/213/1/012019

[33]. M.D. Sakhnenko, M.V. Ved', I.Yu. Ermolenko, Yu.K. Hapon, M.O. Kozyar, *Mater Sci.* 52 (2017) 680–686. DOI: 10.1007/s11003-017-0009-7

[34]. N. Ćirović, P. Spasojević, L. Ribić-Zelenović, P. Mašković, M. Spasojević, *Sci. Sinter.* 47 (2015) 347–365. DOI: 10.2298/SOS1503347C

[35]. I.Y. Yermolenko, M.V. Ved', A.V. Karakurkchi, N.D. Sakhnenko, Z.I. Kolupaieva, *Voprosy khimii i khimicheskoi tekhnologii* [Issues of Chemistry and Chemical Technology] 2 (III) (2017) 4–14

[36]. A.B. Sagyndykov, Zh.K. Kalkozova, G.Sh. Yar-Mukhamedova, Kh.A. Abdullin, *Tech. Phys.* 62 (11) (2017) 1675–1678. DOI: 10.1134/S106378421711024X

[37]. A.V. Karakurkchi, M.V. Ved', N.D. Sakhnenko, I.Yu. Yermolenko, S.I. Zyubanova, Z.I. Kolupayeva, *Funct. Mater.* 22 (2015) 181–187. DOI: 10.15407/fm22.02.181

[38]. M.O. Glushkova, M.V. Ved, M.D. Sakhnenko, *Mater Sci.* 49 (2013) 292–297. DOI: 10.1007/s11003-013-9613-3